

Photo-electrical Characterization of New CuAlNi/n-Si/Al Schottky Photodiode Fabricated by Coating Thin-film Smart Material

Oktay KARADUMAN¹, Canan Aksu CANBAY^{2*}

¹ Department of Physics, Science Faculty, Firat University, Elazig, TURKEY

¹ o.karaduman@firat.edu.tr, ^{2*} caksu@firat.edu.tr

(Geliş/Received: 26/04/2022;

Kabul/Accepted: 02/08/2022)

Abstract: Micro/nano scale thin-film shape memory alloys (SMAs) have been used in many different miniaturized systems. Using them as thin-film metal components in fabrication of Schottky photodiodes has started a few years ago. In this work, a new SMA-photodiode device with CuAlNi/n-Si/Al structure was produced by coating nano-thick CuAlNi SMA film onto n-Si wafer substrate via thermal evaporation. The photoelectrical I-V, C-V and I-t photodiode signalization tests were performed under dark and varied artificial light power intensities in room conditions. It was observed that the new device exhibited photoconductive, photovoltaic and capacitive behaviors. By using conventional I-V method, the diode parameters such as electrical ideality factor (n), Schottky barrier height (ϕ_b) and rectification ratio (RR) of the produced photodiode for the condition of dark environment were computed as 12.5, 0.599 eV and 1266, respectively. As good figure of merits, the photodiode's performance parameters of responsivity (R_{ph}), photosensitivity (%PS) and specific detectivity (D^*) maxima values determined for at -5 V reverse voltage bias and under 100 mW/cm² of light power intensity condition are as 0.030 A/W (or 30 mA/W), 18693 and 1.33×10^{10} Jones, respectively. The current conduction mechanism analysis revealed that the space charge limited conduction (SCLC) mechanism is the dominant current conduction mechanism. By the drawn reverse squared C²-V plots, the values of diffusion potential (V_d), donor concentration (N_D), Fermi level (E_F) and also barrier height (ϕ_b) were determined for the SMA-photodiode. The results indicated that the new SMA-photodiode device can be useful in optoelectronic communication systems and photosensing applications.

Keywords: Schottky photodiode, thin-film shape memory alloy, space charge limited current, photosensitivity, detectivity.

İnce Film Akıllı Malzeme Kaplamasıyla Üretilen Yeni CuAlNi/n-Si/Al Schottky Fotodiyotunun Foto-elektriksel Karakterizasyonu

Öz: Mikro/nano ölçekli ince-film şekil hafızalı alaşımlar (ŞHA'lar) birçok farklı minyatürize sistemde kullanılmıştır. Bunların Schottky fotodiyotların üretimlerinde ince-film metal bileşenleri olarak kullanılmaları da henüz birkaç yıl önce başlamıştır. Bu çalışmada, termal buharlaştırma ile n-Si yonga üzerine nano-kalınlıklı CuAlNi ŞHA film kaplanarak CuAlNi/n-Si/Al yapısı şeklinde yeni bir ŞHA-fotodiyot aygıtı üretilmiştir. Fotoelektriksel I-V, I-t ve C-V fotodiyot karakterizasyon testleri oda sıcaklığında, karanlıkta ve farklı yapay ışık gücü yoğunluklarında gerçekleştirilmiştir. Yeni aygıtın fotoiletken, fotovoltajik ve kapasitif davranışlar sergilediği gözlemlenmiştir. Geleneksel I-V yöntemi kullanılarak, üretilen fotodiyotun karanlık ortam koşulu için elektriksel idealite faktörü (n), Schottky engel yüksekliği (ϕ_b) ve doğrultma oranı (RR) gibi diyet parametreleri sırasıyla 12.5, 0.599 eV ve 1266 olarak hesaplanmıştır. İyi başarımlı değerleri olarak, fotodiyotun performans parametrelerinden responsivite (R_{ph}), fotosensitivite (%PS) ve spesifik dedektivite (D^*) parametrelerinin maksimum değerleri -5 V ters beslem voltajında ve 100 mW/cm² ışık gücü yoğunluğu koşulunda belirlenmiş olup sırasıyla 0.030 A/W (veya 30 mA/W), 18693 ve 1.33×10^{10} Jones şeklindedir. Akım iletim mekanizması analizi, uzay yükü sınırlı iletim (SCLC) mekanizmasının baskın akım iletim mekanizması olduğunu ortaya koymuştur. Çizilen ters kare C²-V grafikleri ile, ŞHA-fotodiyot için donör konsantrasyonu (N_D), difüzyon potansiyeli (V_d), Fermi seviyesi (E_F) ve ayrıca bariyer yüksekliği (ϕ_b) değerleri belirlendi. Sonuçlar, yeni üretilen ŞHA-fotodiyot aygıtının optoelektronik iletişim sistemlerinde ve fotosensör uygulamalarında faydalı olabileceğine işaret etmiştir.

Anahtar kelimeler: Schottky fotodiyot, ince-film şekil hafızalı alaşım, uzay yükü sınırlı akım, fotosensitivite, dedektivite.

1. Introduction

Shape memory alloys (SMAs) are a unique smart materials group which have been extensively studied and are ever-increasingly used in many technological and industrial applications [1–11] today due to the shape memory effect (SME) and superelasticity (SE) properties [2] of these highly functional smart alloys. SME is a shape remembering or strain recovery mechanism that occurs as a macroscopic geometric shape change of a SMA when its temperature is changed after mechanically deformed. Such a macro-shape change is a sum of all micro-

* Corresponding author: caksu@firat.edu.tr. ORCID Number of authors: ¹ 0000-0002-6947-7590, ² 0000-0002-5151-4576

crystallographic changes occurring in SMA by an atomically diffusionless and isothermal solid-solid phase transformation called as martensitic transformation (MT). It occurs between two different solid phases existing at different temperatures called as martensite (product or cold) phase and austenite (parent or hot) phase. NiTi, Cu-based and Fe-based SMAs are three main group of SMAs. Among these the equiatomic NiTi SMAs are the most commercially used ones due to the superior SME and SE properties, albeit they are expensive. Therefore, the cheaper Cu-based SMAs plus with higher thermal and electrical conductivity values than NiTi ones have attracted researchers and been studied to improve them for developing alternative to NiTi SMAs [12–19].

Micro or nano sized thin film shape memory alloys (SMAs) have been already used in many different micro and nano electromechanical systems (M/NEMS) such as microactuators, microvalves, micropumps and mass, temperature or force sensors [1,6,7,10,11,20–30]. SMA thin films can be patterned with standard lithography techniques thus they can be integrated into MEMS devices [30]. Apart from usual thermomechanical MEMS actuator and sensors, coating of thin film SMAs as metal contact layers on semiconductor (silicon) wafers in Schottky diodes have been started in 1990's [25,31,32]. Since a few years ago, photodiodes were also produced by coating Cu-based SMA thin films on silicon wafers [23,28,33–36] for the first time and good photodiode performances, photocapacitance and current rectifying and other diode properties were achieved. For example, in one [23] of these works made on fabrication of a Au/CuAlMnV/n-Si/Al diode by using a nano-layer of thin film CuAlMnV shape memory alloy they reported that a 6.3 of ideality factor, a 0.54 eV of barrier height in dark condition, a photocurrent sensitive to illumination intensity and linearly increases with increasing illumination intensity and also a capacitance and a conductivity varying strongly with frequency changes. In another work [33] made on a CuAlMnNi/p-Si/Al quadrant photodiode a 2.72 of ideality factor, a 0.65 eV of barrier height for dark condition, and similar light-induced photocurrent generation and frequency dependent capacitance characteristics were reported. In else one [34] made on CuAlMn±Cr/p-Si/Al photodiodes, a minimum 2.03 value of ideality factor, the maxima 12480.33 of rectification ratio and 0.59 eV of barrier height values, and similar photosensitive and capacitive features were reported. The thin film SMAs used in these kind of works were Cu-based SMAs because their thermal and electrical conductivities are higher than NiTi SMAs withal Cu-based SMAs are proper for silicon in terms of metal work function, too, which is important in building a semiconductor/metal contact.

However, the number of these new research works made on SMA-photodiodes are very few and plainly insufficient. Also the spectrum of the types and alloy compositions of SMAs used as thin films in these works are still very diminutive. So, there are more and more explorative works that can be done upon such kind photodiodes with thin film SMA layer components. Mostly because the work function of SMAs, interface and photodiode/diode characteristics are sensitively depended on the type and composition of SMAs used as thin films in these kind of photodiodes. Works with different Cu-based SMAs, different alloy compositions or other many combinations of components and conditions have not been made yet. Being inspired by these motivations, in the study presented here, it is aimed to fabricate and characterize a nano thin film shape memory alloy layered CuAlNi/n-Si/Al photodiode with using a different type of shape memory alloy (a CuAlNi HTSMA) than the ones reported in the literature. Also, due to their inexpensive production cost and high resistance to the degradation of functional properties that occurred during the aging processes [12], the CuAlNi SMAs are one SMA group among the two most commercially used Cu-rich SMAs (the other is CuZnAl group), which is important in terms of practicality and accessibility in the related potential photodiode applications.

In this work, a new SMA-photodiode structured as Schottky type CuAlNi/n-Si/Al junction contact was produced by coating of CuAlNi SMA on an n-type silicon (n-Si) via thermal evaporation and by performing the photoelectrical I-V, I-t and C-V characterization measurements the photodiode properties of the device were revealed.

2. Experimental

In this experimental research study, the CuAlNi shape-memory-alloy with an atomical Cu-25.04Al-3.88Ni (at%) chemical composition from using the powders of the highly pure (~99.9) Cu, Al, and Ni alloying elements was previously fabricated as ribbons (with ~5 mm wideness and 15 µm thickness) by melt spinning method without applying a post-homogenization process. More details about the production process and thermo-structural DSC, DTA and XRD characterization results of this CuAlNi high temperature SMA (HTSMA) were given in the previous work [37]. In the fabrication process of the new Schottky type CuAlNi/n-Si/Al metal/semiconductor (MS) junction contact photodiode for coating CuAlNi SMA and Al metal driblets in sequence onto the back (ohmic) and polished front (Schottky) sides of an n-Si wafer a Nanovak labeled thermal evaporation system was operated. Before making coatings for building these MS contacts, the n-Si wafer and metal driblets were cleaned via the standard cleaning treatment. This standard cleaning method consists of washing by ultrasonic bathing

sequentially in media of water (distilled), acetone and then ethyl alcohol (for 5 min in each medium), etching the wafer in (1:10 ml) HF:H₂O solution for ~30 s, washing by distilled-water and desiccating it by spraying nitrogen gas. Under a chamber pressure of 2×10^{-6} Pa in evaporator, the backside of the wafer was coated by 150 nm thickness of Al metal film layer and thus the ohmic n-Si/Al contact structure was built and then this was annealed under constant nitrogen gas flow at 570 °C for 5 min long for making diffusion of n-Si and Al surfaces one another. Then by shadowing the front face of the n-Si wafer with a proper splashy mask with small circular holes, the Schottky top diode contact on the bright front face of n-Si was built by evaporating a CuAlNi SMA metal piece to form 150 nm thickness of a thin film CuAlNi SMA layer. Each one of the diode's top-contact CuAlNi spots marked off by mask holes has an area (A) of 0.785×10^{-2} cm². By using FYM-7000 and FYM-9000 model FYTRONIX lable Solar Simulator electronic characterization systems, the photo-electrical characterization of the produced device was carried out by performing current-voltage (I-V), capacitance-voltage (C-V) and current-time (I-t) measurements under dark and varied artificial day light power intensities in room conditions. The fabricated SMA-photodiode structure was schematically presented in Figure 1.

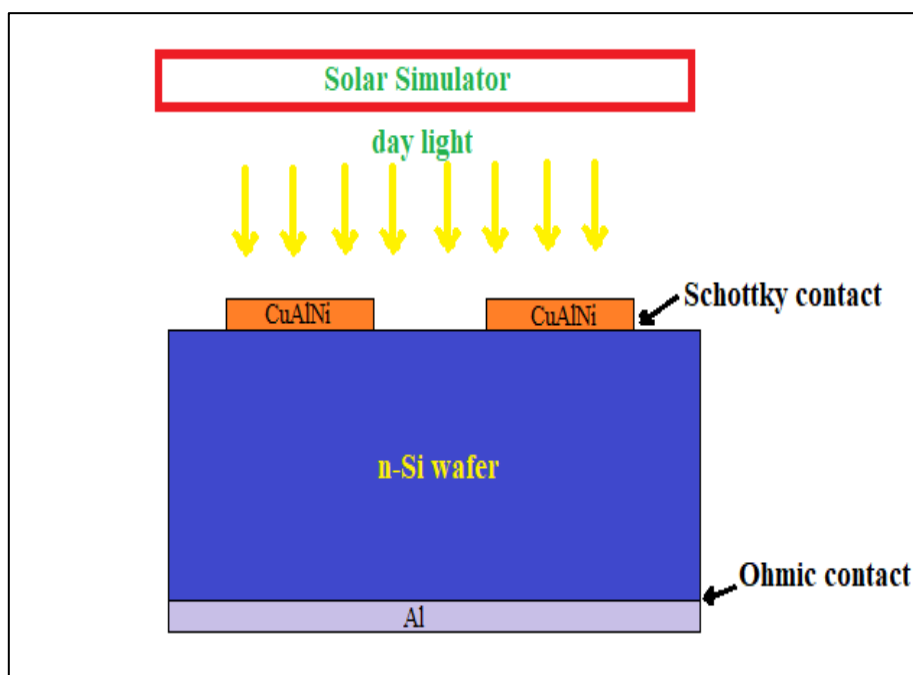


Figure 1. A schematic presentation of the fabricated CuAlNi/n-Si/Al SMA-photodiode structure.

3. Results and Discussions

The characterization measurements findings obtained for CuAlNi shape memory alloy and CuAlNi/n-Si/Al photodiode were given below as following in succession.

The DSC curve of the ribbon CuAlNi alloy obtained at a single heating-cooling rate (25 °C/min) is presented as both DSC heat-flow (mW) vs. temperature (°C) and heat flow vs. time (min.) graphics in Figure 2-a and -b, respectively. On these graphics of same DSC curve at between ~192 °C and ~293 °C, the downward endothermic peak seen on heating the alloy and the correspondent upward exothermic peak seen on cooling the alloy indicate the reverse martensite-to-austenite (M→A) and direct austenite-to-martensite (A→M) martensitic phase transformations, respectively. This reversible solid-solid phase reaction demonstrates that the CuAlNi alloy has a shape memory effect property. The alloy is a high temperature SMA due to its transformation temperatures are above 100 °C.

The thermodynamical parameters such as the start and finish temperatures (M_s , M_f , A_s and A_f) of the martensite and austenite phases, hysteresis gap ($A_s - M_f$), maximum M→A transformation peak temperature (A_{max}), equilibrium temperature (T_0), and the enthalpy change (ΔH) and entropy change (ΔS) values related to the M→A transformation of the CuAlNi alloy were listed in Table 1. Among these values, the T_0 and $\Delta S_{M \rightarrow A}$ values were determined by using $T_0 = 0.5 \times (A_f + M_s)$ and $\Delta S_{M \rightarrow A} = \Delta H_{M \rightarrow A} / T_0$ relations [15,28].

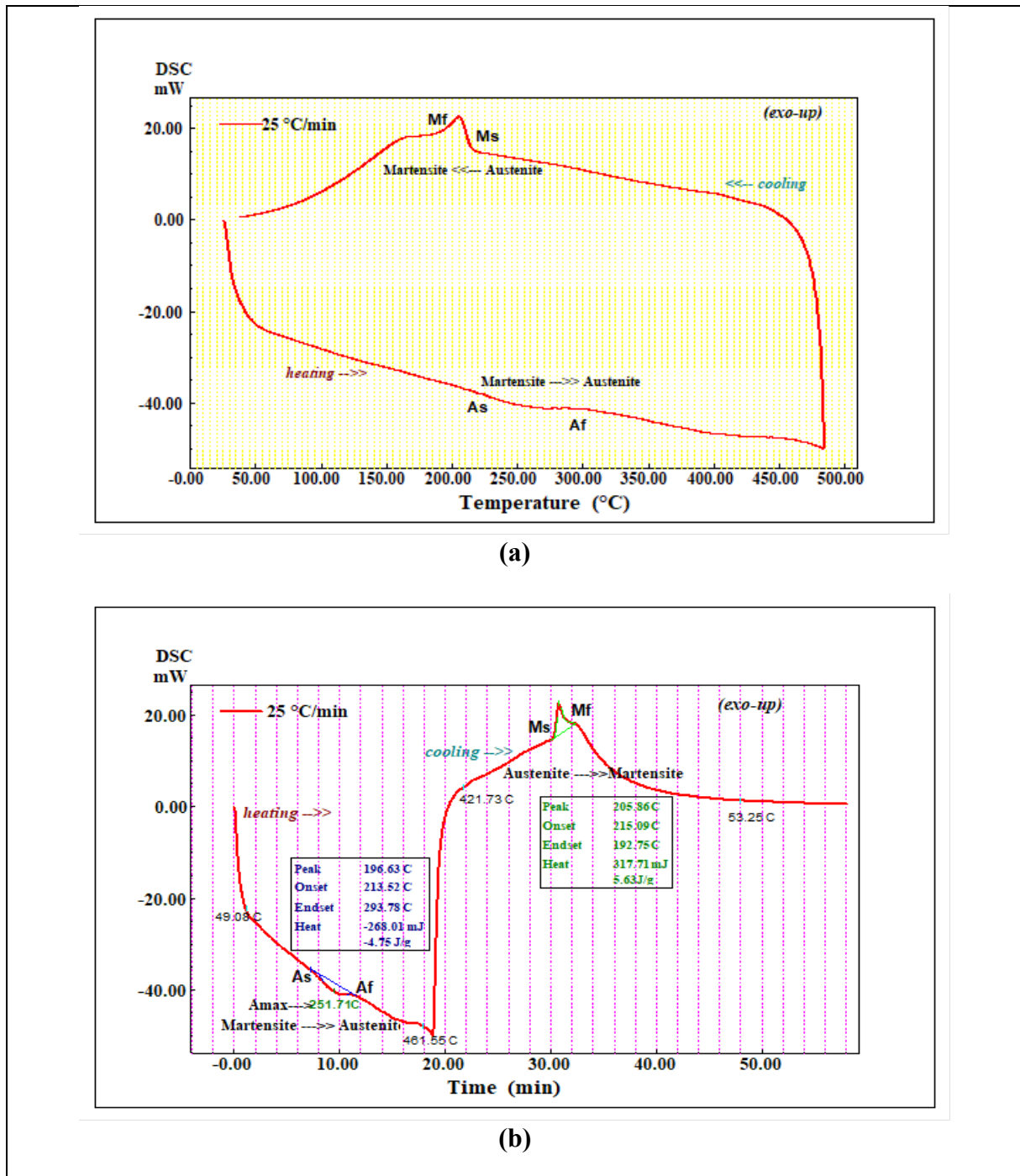


Figure 2. The DSC curve of the CuAlNi alloy as on x-axis of a) temperature and b) time.

Table 1. The thermodynamical parameters and martensitic transformation temperatures of the CuAlNi alloy.

Heating/cooling rate (C/min)	A_s (°C)	A_r (°C)	A_{max} (°C)	M_s (°C)	M_r (°C)	A_s-M_r (°C)	T_0 (°C)	$\Delta H_{M \rightarrow A}$ (J/g)	$\Delta S_{M \rightarrow A}$ (J/g°C)
25	213.52	293.78	251.71	215.09	192.75	20.77	254.44	4.75	0.01867

The thermal response cycling heating/cooling pattern of the alloy in high temperature region shown as DTA curve obtained between room temperature and 900 °C by 25 °C/min of heating-cooling rate can be seen in Figure 3. On this DTA curve, the sequential phase transitions of $\beta 1'(+\gamma 1')$ \rightarrow $\beta 1$ (or B1) \rightarrow $\beta 2$ (metastable) \rightarrow $\gamma 2+\alpha$ (precipitation) \rightarrow eutectoid reaction \rightarrow B2(ordered) \rightarrow A2 (disordered) were observed on heating the alloy, which transitions are a common similar behavior of copper-based shape memory alloys [15,19,38].

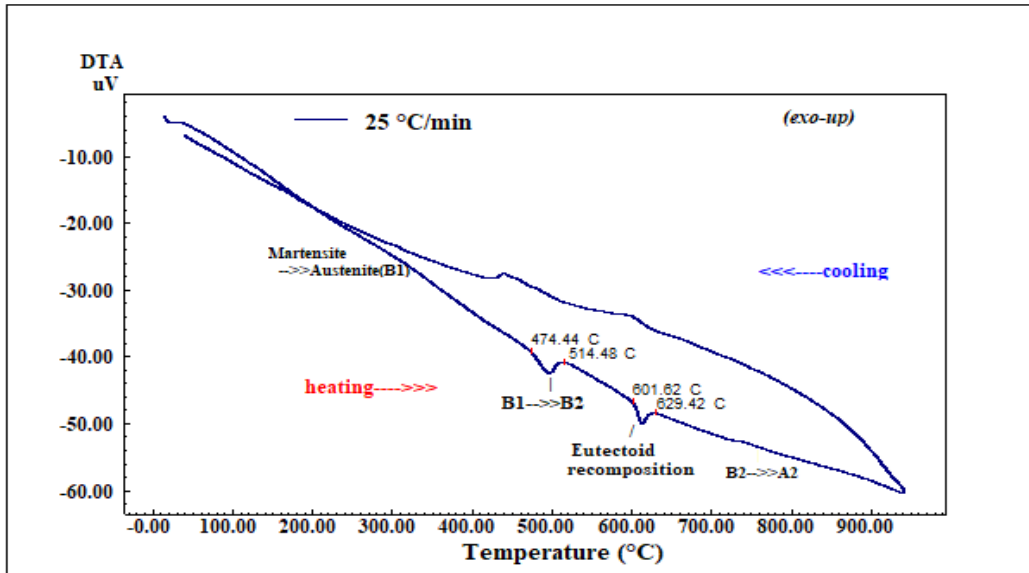


Figure 3. The DTA curve of the CuAlNi shape memory alloy.

The X-ray diffraction pattern of the CuAlNi alloy obtained at room temperature by using $\text{CuK}\alpha$ radiation is presented in Figure 4. As seen on this crystallograph, the martensite phase of $\gamma 1'(211)$ peak is the highest and this peak with the other $\gamma 1'$ and $\beta 1'$ martensite peaks [15,16,28,33,37] indicate the formation of a structure which is underlying mechanism of shape memory effect property of the CuAlNi alloy. The $\beta 1$ and $\gamma 1$, $\gamma 2$, and α -Cu precipitates are the other appeared peaks on the pattern [37]. All of these many small XRD peaks demonstrate that the CuAlNi alloy has a highly polycrystalline structure caused from not making a post-heat-treatment (homogenization) after obtaining ribbon alloy by melt spinning process.

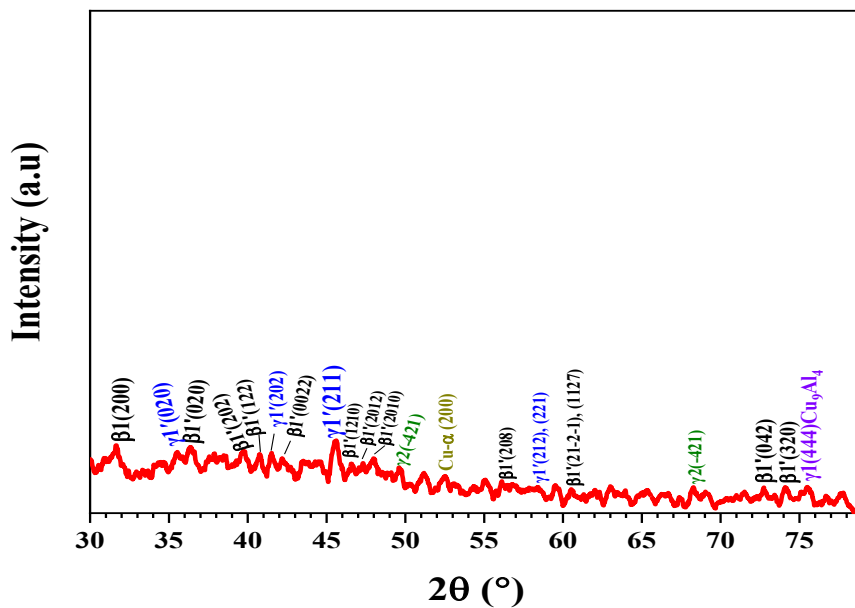


Figure 4. The XRD diffraction pattern CuAlNi alloy.

The photo-electrical I - V graphics of the novel CuAlNi/n-Si/Al photodiode as in semi-log mode obtained under darkness and varied step-increasing artificial day light power intensity conditions are presented in Figure 5. As seen on these plots, the SMA-photodiode rectifies the current; it lets current to flow under forward bias and does not under reverse bias except a low leakage (saturation) current under all conditions. It also shows acute photoconductive photosensitiveness under the all light conditions by crescendo photocurrents in reverse bias current [23,28,33,35,39]. This photocurrent generation and raise in the negative voltage (reverse) bias by light exposure confirms that the fabricated photodevice has photodiode properties. This photocurrent generation occurs by excitation of the valance band electrons by the absorbed incoming photons with enough energies ($h\nu \geq E_g$) beamed from the the solar simulator I-V measuring device. The photo-excited electrons leave holes behind when they pass to the conduction band and this photoelectrical phenomenon (electron-hole pair generation) is named as the photoelectric effect. The reverse bias current in dark is seen as some zig-zag noisy but the illuminated reverse bias currents are highly stable. Moreover, the forward bias current is seen also increased by the effect of light power. All of these findings indicate that the new device has good photoconductive and photovoltaic properties.

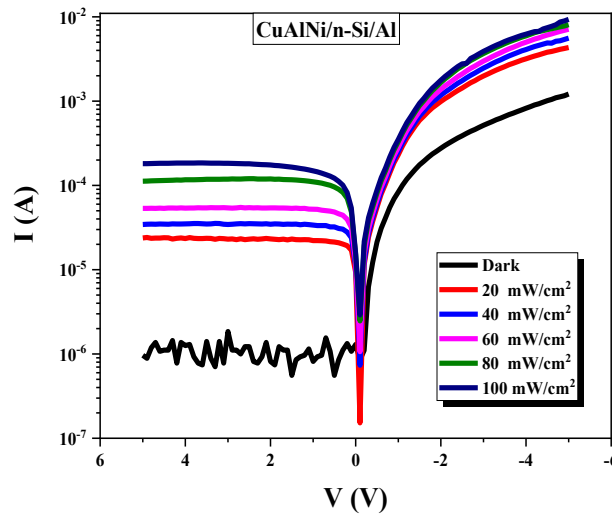


Figure 5: The semi-log I - V plots of the fabricated CuAlNi/n-Si/Al SMA-photodiode obtained under the conditions of dark and different light power intensities.

One of the electrical diode parameters is current rectifying exponent, RR. This ratio is the rate of the absolute current values at a definite absolute-equal negative and positive voltage ($\pm V$) couple. It was found by using $RR_{\pm V} = I_V/I_{-V}$ formula [28]. The value of RR for the SMA-photodiode at ± 5.0 V was determined as 1266 for dark condition and 52 for 100 mW/cm² of light power condition. Close RR values were reported in some other similar works [28, 34,36]. Generally, I - V plot at low voltages of forward bias is linear, however when the applying voltage is raised, deviations from this linearity occurs mainly by the impact of the interfacial layer, interface states (in CuAlNi/n-Si interface) and series resistance (R_s) [40].

For a Schottky (photo)diode the relationship between current and voltage elucidated by the conventional thermionic emission (TE) charge transport mechanism theory is defined by the equation [28,41] (for $V > 3kT/q$ condition) given as below;

$$I = I_0 \exp\left(\frac{q(V-IR_s)}{nkT} - 1\right). \quad (1)$$

where; k refers to the Boltzmann constant, $V-IR_s$ stands for the voltage that drops across the metal-semiconductor junction diode, q is charge of electron, T is temperature ($T= 300$ K), n refers to the unitless ideality factor parameter of the diode, I_0 is the reverse saturation current obtained from the intersecting of linear segment of $\ln(I)$ - V plot in forward bias region. The saturation current I_0 is expressed as below;

$$I_0 = AA^*T^2 \exp\left(-\frac{q\phi_b}{kT}\right) \quad (2)$$

where; ϕ_b refers to the Schottky barrier height (SBH) of the CuAlNi/n-Si/Al SMA-photodiode (at $V=0$), A^* is Richardson invariant (for n-Si the theoretical value of A^* is $112 \text{ A}\cdot\text{cm}^{-2}\text{K}^{-2}$) [41,42], and A stands for the CuAlNi top-contact diode area ($=0.785 \times 10^{-2} \text{ cm}^2$) of the manufactured CuAlNi/n-Si/Al photodiode. The n ideality factor values were computed by substituting the slope quantities of the linear fragments of the $\ln(I)$ - V plots (in the positive biased voltage side) of the SMA-photodiode in the following formula;

$$n = \frac{q}{kT} \left(\frac{dV}{d(\ln I)} \right) \quad (3)$$

The ideality factor n of the CuAlNi/n-Si/Al photodiode was computed as 12.5 for darkness condition and 13.3 for 100 mW/cm^2 power of illuminated condition and these n values are higher than the ideal value ($n=1$). The deviations occurring in n values from the value of ideal one (1) are attributed to the influences of non-uniform distribution of charges in the interface, interface states, impurities, the inhomogeneity of SBH across the junction [28,43,44]. The value of the SBH (ϕ_b) for the signalized photodiode consisting thin-film CuAlNi SMA top-layer can be calculated by using the following formula [28];

$$\phi_b = \frac{kT}{q} \ln \left(\frac{AA^*T^2}{I_0} \right) \quad (4)$$

The ϕ_b value for the CuAlNi/n-Si/Al photodiode was computed as 0.599 eV for dark condition and 0.566 for 100 mW/cm^2 power of illuminated condition. As seen, the n , ϕ_b and RR values of the produced SMA-photodiode are found changed by the light effect. These changes occurred most probably because of the carrier generation-recombination induced by the incident luminous effect and the effect of interface states in the interface of CuAlNi/n-Si Schottky contact [28,45].

One of the most important figure of merits of a photodiode is its responsivity (R_{ph}) parameter that reveals the photo-detecting performance of a photodiode viz; how that device absorbs and reacts to the incident light. R_{ph} is the rate of the generated output photocurrent to the power of incoming light and can be calculated by using $R_{ph}=I_{ph}/P \cdot A_{eff}$ formula [46], where I_{ph} stands for the net photocurrent ($I_{ph} = I_{light} - I_{dark}$), P refers to the incoming light power intensity, and A_{eff} is the effectively enlightened area (6 mm^2) of the produced photodiode. For at -5 V of reverse bias, the net photocurrent R_{ph} responsivity values of the manufactured SMA-photodiode under 20 mW/cm^2 and 100 mW/cm^2 of light power intensities were found as 0.019 A/W and 0.030 A/W (or 19 mA/W and 30 mA/W), respectively. These responsivity values are found similar to those reported in some recent works [46,47]. Moreover, in this work, even higher responsivity values could be achieved by applying larger light power intensities than 100 mW/cm^2 as far as the limit of the SMA-photodiode device [28].

Another photodiode parameter is the photosensitivity parameter, which is defined as a measure of the photodiode's ability to absorb incoming light. It is a unitless parameter and represented as PS or percent %PS. The better the photodiode can absorb light, the greater its photosensitivity. A formula [28,44] to determine the %PS photosensitivity parameter is given as $\%PS = [(I_{ph} - I_d) \times 100] / I_d$, where I_d is dark current. For at -5 V and under 100 mW/cm^2 light power condition, the photosensitivity %PS value of the SMA-photodiode was found as 18693 and this value is consistent with some recent literature values [28,44,48].

Specific detectivity (D^*) is another figure of merit for a photodiode and it is defined as the weak light (signal) detection capability of a photodiode [28]. For shot-noise limit condition, the detectivity D^* value of the device normalized by the effective diode area (A_{eff}) can be calculated by $D^*=R_{ph}/(2qI_d/A_{eff})^{1/2}$ formula [28,49], where q is electron charge. The higher detectivity a photodiode has, the more sensitively it can detect weak signals. The photodiodes with high detectivities can be used in optoelectronic communication systems. For at -5 V and under 100 mW/cm^2 light power condition, the D^* value of the SMA-photodiode was calculated as 1.33×10^{10} Jones and this value is in accordance with some recently reported literature values [28,44,48,49].

In MS Schottky contacts the current is not conducted by thermionic emission mechanism at forward bias due to the absence of a potential barrier and depletion layer. The current conduction mechanisms that must be dominant in the produced SMA-photodiode during at forward voltage bias and under dark condition were investigated by making SCLC (space charge limited current) analysis [50–52], which is made according to $I \propto V^m$ power law relationship. To make this analysis, under dark condition the forward bias $\ln(I)$ - $\ln(V)$ graphic of the produced SMA-photodiode was drawn and given in Figure 6. The slope (m) values found for the linear parts of this graphic are defined by the current conduction mechanisms regions as; the I.Region ($m < 1$) is electron tunneling region due to low voltages, (the II.Region ($m=1$, $I \propto V$) is ohmic conduction but not found here so instead) the II.Region ($m=2$, $I \propto V^2$) is trap free SCLC conduction (all traps are filled) and this region is also called as super ohmic or

super linear conduction, the III.Region ($m > 2$, $I \propto V^m$) is SCLC with trap effect and lastly the IV.Region ($1 < m < 2$, $I \propto V^{-1.5}$ or $I \propto \exp(V)$) is SCLC based on recombination-tunneling mechanisms.

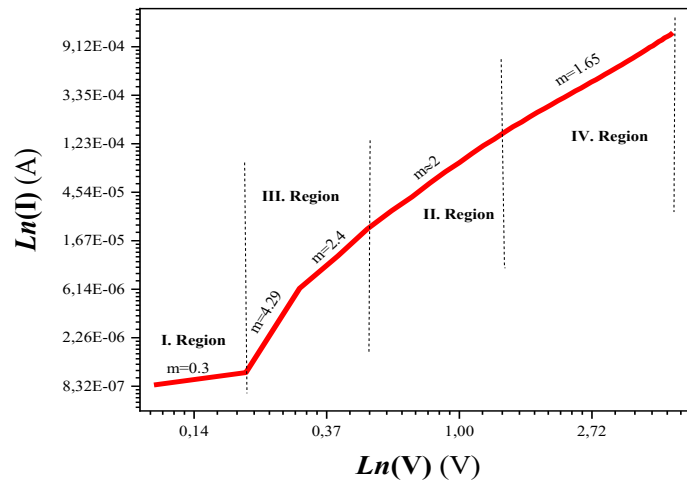


Figure 6. The regions of dominant current conduction mechanisms on the double logarithmic $Ln(I)$ - $Ln(V)$ current-voltage graphic of the CuAlNi/n-Si/Al SMA-photodiode at forward bias and under dark.

To set apart of carrier charges generated by the photovoltaic effect of the SMA-photodiode the dynamic (time-dependent) photocurrent response also called as transient photocurrent (TPC) measurement was performed on SMA-photodiode. The obtained TPC patterns of the novel photodiode under increasing light power intensities were given in Figure 7. On these patterns, upon the light is turned on each time, the photocurrent rapidly ascends a higher altitude due to the light induced generation of the excess charge carriers and remains barely constant till the light off. Each time the light is put out, the photocurrent comes down to its initial level like rapidly again. Such swift downfalls on these curves occur due to the excess carriers and trapped carriers recombination in the deep levels [28,33,53].

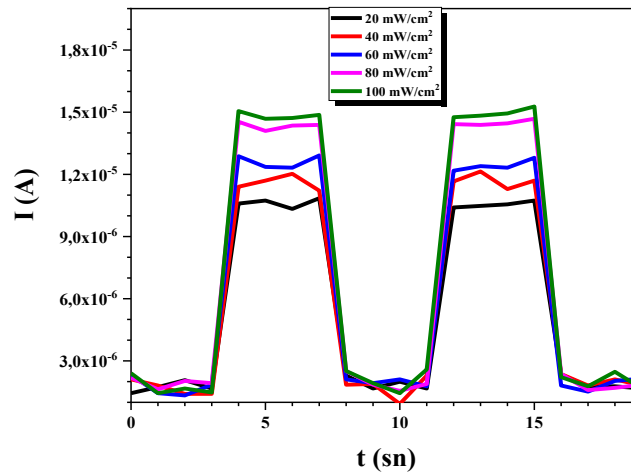


Figure 7. The characteristic photoreactive time-dependent I-t (TPC) curves of the produced CuAlNi/n-Si/Al photodiode as its response to the different P (mW/cm^2) light power intensities.

The capacitance-voltage (C-V) curves of the photodiode obtained at different step frequencies are presented in Figure 8 (due to the opposite probe poles used in the C-V measurement the left voltage side in this figure is actually reverse bias region). According to these C-V curves, the capacitance of the SMA-photodiode changes by change of frequency and applied voltage [28, 33-36, 54-56]. The higher frequency, the lower capacitance. Because the electrons cannot chase the ac current at high frequencies and therefore they don't contribute to the total

capacitance at high frequencies [23, 54-56]. The capacitance of the photodiode becomes zero in the forward bias region at all frequencies.

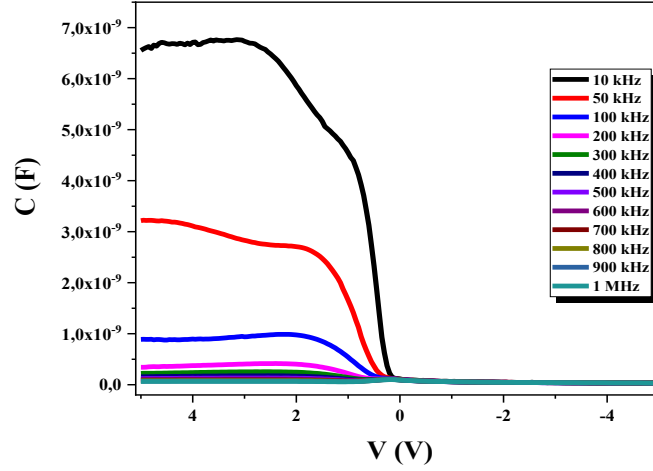


Figure 8. The characteristic capacitance-voltage (C - V) curves of the produced CuAlNi/n-Si/Al photodiode obtained at different frequencies.

By plotting the inverse squared capacitance-voltage (C^{-2} - V) curves of the SMA-photodiode as given in Figure 9 some other electrical parameters can be determined at the reverse bias (negative voltage) region. The values of these parameters were calculated by using the linear fit value obtained from the graphic at 1 MHz. The capacitance of depletion layer is expressed by the formula [28] given as below;

$$C^{-2} = \frac{2(V_d + V)}{q\epsilon_0\epsilon_s A^2 N_D} \quad (5)$$

where; N_D is concentration of non-compensated ionized donor atoms, V_d refers to diffusion potential, A is diode area, q is electron charge, ϵ_s (=11.8 for n-Si) is permittivity of the semiconductor and ϵ_0 is permittivity of space. The values of N_D and V_d are determined by the slope and linear extrapolation of the C^{-2} - V plot to the x -axis (voltage). The donor concentration N_D can be calculated by the following formula [28];

$$N_D = \frac{2}{q\epsilon_0\epsilon_s A^2} \left[\frac{d(C^{-2})}{dV} \right]^{-1} \quad (6)$$

The values of N_d and V_d at 1 MHz were determined as 1.25×10^{15} [28] and 0.875 V, respectively. Plus, the Schottky barrier height ϕ_b can be also calculated from the C^{-2} - V method by using the formula given as below;

$$\phi_b = \frac{V_d}{n} + \frac{kT}{q} \ln \left(\frac{N_C}{N_D} \right) \quad (7)$$

where; N_C refers to the effective density of states in the conduction band of n-Si substrate ($N_C = 2.8 \times 10^{19} \text{ cm}^{-3}$). By this method, the value of ϕ_b was found as 0.330 eV and this value was found lower than the conventional 0.599 eV value found by I - V method. This difference is due to the coating CuAlNi alloy metal layer onto n-Si without use of an insulator interlayer which makes the capacitance of the produced device lower than those of the diodes (MIS) with insulator interlayer [28]. Moreover, the effective Fermi energy (E_F) was determined as 0.260 eV by using $E_F = \phi_b - (V_d/n)$ formula, and it was found as 0.529 eV from the conventional I - V method [28].

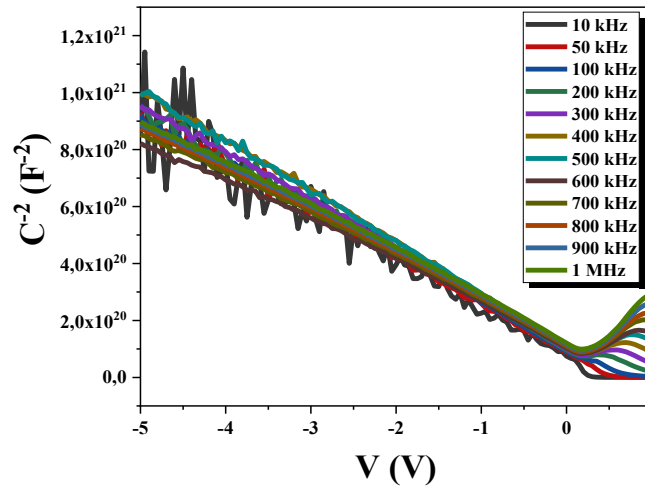


Figure 9. Multiple C^2 - V graphs of CuAlNi/n-Si/Al SMA-photodiode at different frequencies.

4. Conclusions

In this work, the new MS Schottky type CuAlNi/n-Si/Al SMA-photodiode was successfully fabricated by coating nano-thick CuAlNi shape memory alloy thin film as top diode metal contact onto n-Si substrate using thermal evaporation method. The CuAlNi alloy was classified as a high temperature shape memory alloy with a high polycrystalline structure including martensite phases. The photo-electrical I-V, I-t and C-V measurements were carried out for characterization of the SMA-photodiode device. The electrical ideality factor, Schottky barrier height and rectification ratio diode parameters of the produced device were determined from the I-V method as 12.5, 0.599 eV and 1266, respectively. The high ideality factor deviated from unity was caused mainly from the presence of interface states, non-uniform distribution of the interface charges and barrier inhomogeneity across the CuAlNi/n-Si contact. The SCLC current conduction mechanisms were found as the dominant current conduction mechanisms at forward bias and in dark condition. The produced SMA-photodiode showed remarkable photoconductive and photovoltaic profile and very well photodiode figure of merits such as a huge photosensitivity (%PS) value of 18693, a specific detectivity of $\sim 10^{10}$ Jones and a responsivity of 0.030 A/W by the effect of applied artificial solar light. These merits show that the produced SMA-photodiode can be used in photosensor and optical communication systems. It was observed that the electrons cannot follow the applied ac voltage at the high frequencies of C-V tests made on the SMA-photodiode. All of the results showed that this novel CuAlNi/n-Si/Al photodiode can be potentially used in photodiode, photosensor, optoelectronic communication systems, photovoltaic etc. applications and also in M/NEMs applications where light-induced actuating-sensing mechanism is based on.

Acknowledgements

This research work is a part of Ph.D. thesis works of Oktay KARADUMAN supervised by Prof. Dr. Canan Aksu CANBAY at Firat University, Faculty of Science, Department of Physics and was financially supported by FÜBAP, Project No: FF.21.14. O.K. wrote the article, implemented the experiments and C.A.C. wrote the article.

References

- [1] J. Mohd Jani, M. Leary, A. Subic, M.A. Gibson, A review of shape memory alloy research, applications and opportunities, *Materials and Design*. 56 (2014) 1078–1113. <https://doi.org/10.1016/j.matdes.2013.11.084>.
- [2] K. Otsuka, C.M. Wayman, *Shape memory materials*, Cambridge University Press, 1999.
- [3] A. Concilio, V. Antonucci, F. Auricchio, L. Lecce, E. (Eds.). Sacco, *Shape Memory Alloy Engineering*, 2nd ed., Elsevier, 2021. <https://doi.org/10.1016/C2018-0-02430-5>.
- [4] J. Ma, I. Karaman, R.D. Noebe, High temperature shape memory alloys, *International Materials Reviews*. 55 (2010) 257–315. <https://doi.org/10.1179/095066010X12646898728363>.
- [5] A. Rao, A.R. Srinivasa, J.N. Reddy, *Introduction to shape memory alloys*, SpringerBriefs in Applied Sciences and Technology. (2015) 1–31. https://doi.org/10.1007/978-3-319-03188-0_1.

- [6] Y.Q. Fu, J.K. Luo, A.J. Flewitt, W.M. Huang, S. Zhang, H.J. Du, W.I. Milne, Thin film shape memory alloys and microactuators, *Int. J. Computational Materials Science and Surface Engineering*. 2 (2009) 208–226. <https://doi.org/10.1504/IJCMSE.2009.027483>.
- [7] P. Krulevitch, A.P. Lee, P.B. Ramsey, J.C. Trevino, J. Hamilton, M. Allen, Thin film shape memory alloy microactuators, 1996. <https://doi.org/10.1109/84.546407>.
- [8] E. Patoor, D.C. Lagoudas, P.B. Entchev, L.C. Brinson, X. Gao, Shape memory alloys, Part I: General properties and modeling of single crystals, *Mechanics of Materials*. 38 (2006) 391–429. <https://doi.org/10.1016/j.mechmat.2005.05.027>.
- [9] J.M. San Juan, M.L. N6, C.A. Schuh, Superelasticity and shape memory in micro- and nanometer-scale pillars, *Advanced Materials*. 20 (2008) 272–278. <https://doi.org/10.1002/adma.200701527>.
- [10] N. Choudhary, D. Kaur, Shape memory alloy thin films and heterostructures for MEMS applications: A review, *Sensors and Actuators, A: Physical*. 242 (2016) 162–181. <https://doi.org/10.1016/j.sna.2016.02.026>.
- [11] I. Stachiv, E. Alarcon, M. Lamac, Shape memory alloys and polymers for mems/nems applications: Review on recent findings and challenges in design, preparation, and characterization, *Metals (Basel)*. 11 (2021) 1–28. <https://doi.org/10.3390/met11030415>.
- [12] S. Najah Saud Al-Humairi, Cu-Based Shape Memory Alloys: Modified Structures and Their Related Properties, in: *Recent Advancements in the Metallurgical Engineering and Electrodeposition*, IntechOpen, 2020. <https://doi.org/10.5772/intechopen.86193>.
- [13] R. Dasgupta, A look into Cu-based shape memory alloys: Present scenario and future prospects, *Journal of Materials Research*. 29 (2014) 1681–1698. <https://doi.org/10.1557/jmr.2014.189>.
- [14] K.K. Alaneme, J.U. Anaele, E.A. Okotete, Martensite aging phenomena in Cu-based alloys: Effects on structural transformation, mechanical and shape memory properties: A critical review, *Sci Afr*. 12 (2021). <https://doi.org/10.1016/j.sciaf.2021.e00760>.
- [15] C.A. Canbay, O. Karaduman, N. Ünlü, S.A. Baiz, İ. Özkul, Heat treatment and quenching media effects on the thermodynamical, thermoelastical and structural characteristics of a new Cu-based quaternary shape memory alloy, *Composites Part B: Engineering*. 174 (2019) 106940. <https://doi.org/10.1016/j.compositesb.2019.106940>.
- [16] O. Karaduman, C. Aksu Canbay, N. Ünlü, S. Özkul, Analysis of a newly composed Cu-Al-Mn SMA showing acute SME characteristics, in: *AIP Conference Proceedings*, American Institute of Physics Inc., 2019. <https://doi.org/10.1063/1.5135437>.
- [17] S.N. Saud, E. Hamzah, T.A. Abu Bakar, A. Abdolahi, Influence of addition of carbon nanotubes on structure-properties of Cu-Al-Ni shape memory alloys, *Materials Science and Technology (United Kingdom)*. 30 (2014) 458–464. <https://doi.org/10.1179/1743284713Y.0000000379>.
- [18] U.S. Mallik, V. Sampath, Influence of quaternary alloying additions on transformation temperatures and shape memory properties of Cu-Al-Mn shape memory alloy, *Journal of Alloys and Compounds*. 469 (2009) 156–163. <https://doi.org/10.1016/j.jallcom.2008.01.128>.
- [19] R.O. Ferreira, L.S. Silva, R.A.G. Silva, Thermal behavior of as-annealed CuAlMnAgZr alloys, *Journal of Thermal Analysis and Calorimetry*. 146 (2021) 595–600. <https://doi.org/10.1007/s10973-020-10002-8>.
- [20] S. Karthick, S. Shalini, S.S. Mani Prabu, K. Suhel, A. Vandan, C. Puneet, S. Manoj Kumar, R. Venkatesh, I.A. Palani, Influence of quaternary alloying addition on transformation temperatures and shape memory properties of Cu–Al–Mn shape memory alloy coated optical fiber, *Measurement: Journal of the International Measurement Confederation*. 153 (2020). <https://doi.org/10.1016/j.measurement.2019.107379>.
- [21] Y. Motemani, P.J.S. Buenconsejo, A. Ludwig, Recent Developments in High-Temperature Shape Memory Thin Films, *Shape Memory and Superelasticity*. 1 (2015). <https://doi.org/10.1007/s40830-015-0041-0>.
- [22] Y.Q. Fu, J.K. Luo, W.M. Huang, A.J. Flewitt, W.I. Milne, Thin film shape memory alloys for optical sensing applications, *Journal of Physics: Conference Series*. 76 (2007). <https://doi.org/10.1088/1742-6596/76/1/012032>.
- [23] C.A. Canbay, A. Tatarođlu, W.A. Farooq, A. Dere, A. Karabulut, M. Atif, A. Hanif, CuAlMnV shape memory alloy thin film based photosensitive diode, *Materials Science in Semiconductor Processing*. 107 (2020) 104858. <https://doi.org/10.1016/J.MSSP.2019.104858>.
- [24] A. Isalgue, V. Torra, J.-L. Seguin, M. Bendahan, J.M. Amigo, V. Esteve-Cano, Shape memory NiTi thin films deposited at low temperature, *Materials Science and Engineering A*. 273–275 (1999) 717–721. [https://doi.org/10.1016/S0921-5093\(99\)00403-7](https://doi.org/10.1016/S0921-5093(99)00403-7).
- [25] J.A. Walker, K.J. Gabriel, M. Mehregany, Thin-film processing of TiNi shape memory alloy, *Sensors and Actuators A: Physical*. 21 (1990). [https://doi.org/10.1016/0924-4247\(90\)85047-8](https://doi.org/10.1016/0924-4247(90)85047-8).
- [26] M. Bendahan, J.L. Seguin, D. Lollman, H. Carchano, New type of Schottky barriers using NiTi shape memory alloy films, *Thin Solid Films*. 294 (1997) 278–280. [https://doi.org/10.1016/S0040-6090\(96\)09230-9](https://doi.org/10.1016/S0040-6090(96)09230-9).
- [27] M. Geetha, K. Dhanalakshmi, S. Jayachandran, I.A. Palani, V. Sathish Kumar, Analysis of actuation characteristics of CuAlNiMn/Polyimide thin film shape memory alloy, *Materials Today: Proceedings*. 46 (2021) 9580–9585. <https://doi.org/10.1016/j.matpr.2020.04.689>.
- [28] C.A. Canbay, O. Karaduman, The photo response properties of shape memory alloy thin film based photodiode, *Journal of Molecular Structure*. 1235 (2021) 130263. <https://doi.org/10.1016/j.molstruc.2021.130263>.
- [29] Q. Pan, C. Cho, The Investigation of a Shape Memory Alloy Micro-Damper for MEMS Applications, *Sensors*. 7 (2007). <https://doi.org/10.3390/s7091887>.

- [30] M. Kabla, E. Ben-David, D. Shilo, A novel shape memory alloy microactuator for large in-plane strokes and forces, *Smart Materials and Structures*. 25 (2016). <https://doi.org/10.1088/0964-1726/25/7/075020>.
- [31] K.R.C. Gisser, J.D. Busch, A.D. Johnson, A.B. Ellis, Oriented nickel-titanium shape memory alloy films prepared by annealing during deposition, *Applied Physics Letters*. 61 (1992) 1632–1634. <https://doi.org/10.1063/1.108434>.
- [32] A.P. Jardine, H. Zhang, L.D. Wasielesky, Investigations into the thin-film fabrication of intermetallic NiTi, *Mat. Res. Soc. Symp. Proc.* 187 (1990) 181–186. <https://doi.org/10.1557/PROC-187-181>.
- [33] C.A. Canbay, A. Tataroglu, A. Dere, A. Al-Ghamdi, F. Yakuphanoglu, A new shape memory alloy film/p-Si solar light four quadrant detector for solar tracking applications, *Journal of Alloys and Compounds*. 688 (2016) 762–768. <https://doi.org/10.1016/J.JALLCOM.2016.07.087>.
- [34] C. Aksu Canbay, A. Dere, K. Mensah-Darkwa, A. Al-Ghamdi, Z. Karagoz Genç, R.K. Gupta, F. Yakuphanoglu, New type of Schottky diode-based Cu–Al–Mn–Cr shape memory material films, *Applied Physics A: Materials Science and Processing*. 122 (2016). <https://doi.org/10.1007/s00339-016-0208-3>.
- [35] C.A. Canbay, A. Tataroğlu, A. Dere, A.G. Al-Sehemi, A. Karabulut, A.A. Al-Ghamdi, F. Yakuphanoglu, Electrical, kinetic and photoelectrical properties of CuAlMnMg shape memory alloy/n-Si Schottky diode, *Journal of Alloys and Compounds*. 888 (2021) 161600. <https://doi.org/10.1016/J.JALLCOM.2021.161600>.
- [36] E. Aldirmaz, A. Tataroğlu, A. Dere, M. Güler, E. Güler, A. Karabulut, F. Yakuphanoglu, Cu-Al-Mn shape memory alloy based Schottky diode formed on Si, *Physica B: Condensed Matter*. 560 (2019) 261–266. <https://doi.org/10.1016/j.physb.2018.12.024>.
- [37] O. Karaduman, İ. Özkul, C.A. Canbay, Shape memory effect characterization of a ternary CuAlNi high temperature SMA ribbons produced by melt spinning method, *Advanced Engineering Science*. 1 (2021) 26–33. <http://publish.mersin.edu.tr/index.php/ades>.
- [38] C.A. Canbay, O. Karaduman, N. Ünlü, İ. Özkul, M.A. Çiçek, Energetic Behavior Study in Phase Transformations of High Temperature Cu–Al–X (X: Mn, Te, Sn, Hf) Shape Memory Alloys, *Transactions of the Indian Institute of Metals*. (2021). <https://doi.org/10.1007/S12666-021-02241-6>.
- [39] E. Aldirmaz, M. Guler, E. Guler, A. Dere, A. Tataroğlu, A.G. Al-Sehemi, A.A. Al-Ghamdi, F. Yakuphanoglu, A shape memory alloy based on photodiode for optoelectronic applications, *Journal of Alloys and Compounds*. 743 (2018) 227–233. <https://doi.org/10.1016/J.JALLCOM.2018.01.380>.
- [40] P. Cova, A. Singh, A. Medina, R.A. Masut, Effect of doping on the forward current-transport mechanisms in a metal–insulator–semiconductor contact to InP:Zn grown by metal organic vapor phase epitaxy, *Solid-State Electronics*. 42 (1998) 477–485. [https://doi.org/10.1016/S0038-1101\(97\)00250-5](https://doi.org/10.1016/S0038-1101(97)00250-5).
- [41] S.M. Sze, K.N. Kwok, *Physics of Semiconductor Devices*, 3rd ed., John Wiley Sons Inc., Hoboken, New Jersey, 2006.
- [42] A. Tataroğlu, F.Z. Pür, The Richardson constant and barrier inhomogeneity at Au/Si 3N4/n-Si (MIS) Schottky diodes, *Physica Scripta*. 88 (2013). <https://doi.org/10.1088/0031-8949/88/01/015801>.
- [43] S. Riazimehr, S. Kataria, J.M. Gonzalez-Medina, S. Wagner, M. Shaygan, S. Suckow, F.G. Ruiz, O. Engström, A. Godoy, M.C. Lemme, High Responsivity and Quantum Efficiency of Graphene/Silicon Photodiodes Achieved by Interdigitating Schottky and Gated Regions, *ACS Photonics*. 6 (2019) 107–115. <https://doi.org/10.1021/acsp Photonics.8b00951>.
- [44] V. Balasubramani, J. Chandrasekaran, T.D. Nguyen, S. Maruthamuthu, R. Marnadu, P. Vivek, S. Sugarthi, Colossal photosensitive boost in Schottky diode behaviour with Ce-V2O5 interfaced layer of MIS structure, *Sensors and Actuators, A: Physical*. 315 (2020). <https://doi.org/10.1016/j.sna.2020.112333>.
- [45] S. Ruzgar, M. Caglar, Fabrication and characterization of solution processed Al/Sn:ZnO/p-Si photodiodes, *Materials Science in Semiconductor Processing*. 115 (2020) 105076. <https://doi.org/10.1016/j.mssp.2020.105076>.
- [46] A.G. Imer, E. Kaya, A. Dere, A.G. Al-Sehemi, A.A. Al-Ghamdi, A. Karabulut, F. Yakuphanoglu, Illumination impact on the electrical characteristics of Au/Sunset Yellow/n-Si/Au hybrid Schottky diode, *Journal of Materials Science: Materials in Electronics*. 31 (2020) 14665–14673. <https://doi.org/10.1007/s10854-020-04029-8>.
- [47] P. Vivek, J. Chandrasekaran, R. Marnadu, S. Maruthamuthu, Fabrication of Illumination-Dependent Cu/p-Si Schottky Barrier Diodes by Sandwiching MoO₃ Nanoplates as an Interfacial Layer via JNSP Technique, (n.d.). <https://doi.org/10.1007/s11664-020-08137-3>.
- [48] V. Balasubramani, J. Chandrasekaran, V. Manikandan, T.K. Le, R. Marnadu, P. Vivek, Upgraded photosensitivity under the influence of Yb doped on V2O5 thin films as an interfacial layer in MIS type Schottky barrier diode as photodiode application, *Journal of Solid State Chemistry*. 301 (2021). <https://doi.org/10.1016/j.jssc.2021.122289>.
- [49] U.Y. Won, B.H. Lee, Y.R. Kim, W.T. Kang, I. Lee, J.E. Kim, Y.H. Lee, W.J. Yu, Efficient photovoltaic effect in graphene/h-BN/silicon heterostructure self-powered photodetector, *Nano Research*. 14 (2021) 1967–1972. <https://doi.org/10.1007/s12274-020-2866-x>.
- [50] F. Gul, A simplified method to determine carrier transport mechanisms of metal-oxide resistive random access memory (RRAM) devices, in: *Materials Today: Proceedings*, Elsevier Ltd, 2021: pp. 6976–6978. <https://doi.org/10.1016/j.matpr.2021.03.274>.
- [51] Z. Çaldıran, M. Şinoforoğlu, Ö. Metin, Ş. Aydoğan, K. Meral, Space charge limited current mechanism (SCLC) in the graphene oxide-Fe3O4 nanocomposites/n-Si heterojunctions, *Journal of Alloys and Compounds*. 631 (2015) 261–265. <https://doi.org/10.1016/j.jallcom.2015.01.117>.
- [52] F.C. Chiu, A review on conduction mechanisms in dielectric films, *Advances in Materials Science and Engineering*. 2014 (2014). <https://doi.org/10.1155/2014/578168>.

- [53] C.A. Arredondo, G. Gordillo, Photoconductive and electrical transport properties of AgInSe₂ thin films prepared by co-evaporation, *Physica B: Condensed Matter*. 405 (2010) 3694–3699. <https://doi.org/10.1016/j.physb.2010.05.068>.
- [54] N. Shiwakoti, A. Bobby, K. Asokan, B. Antony, Temperature dependent dielectric studies of Ni/n-GaP Schottky diodes by capacitance and conductance measurements, *Materials Science in Semiconductor Processing*. 42 (2016) 378–382. <https://doi.org/10.1016/j.mssp.2015.11.010>.
- [55] E. Gürgeç, A. Dıkıcı, F. Aslan, Investigation of structural, electrical and photoresponse properties of composite based Al/NiO:CdO/p-Si/Al photodiodes, *Physica B: Condensed Matter*. 639 (2022) 413981. <https://doi.org/10.1016/j.physb.2022.413981>.
- [56] E. GÜRGENÇ, A. DİKİCİ, F. ASLAN, Production and Characterization of Al/NiO:ZnO/p-Si/Al Composite Photodiodes for Solar Energy Tracking Systems, *Turkish Journal of Science and Technology*. (2022). <https://doi.org/10.55525/tjst.1071332>.